

An Innovative Optimization Algorithm for Precise Estimation of the Optical Efficiency of Heliostat Fields

Prof. Mehmet Sait Söylemez^{a, *} and Ra'ad K Mohammed Aldulaimi^{a,b}

^a Department of Mechanical Engineering, University of Gaziantep, 27310 Gaziantep, Turkey

^b University of Baghdad, Baghdad, Iraq

E-mail: sait@gantep.edu.tr (M.S. Söylemez), rd13434@mail2.gantep.edu.tr (R.K.M. Aldulaimi)

*Corresponding Author, Tel.: +90 342 317 2504; fax: +90 342 360 1104

Received: 25.02.2016 Accepted: 28.06.2016

Abstract- Shading and blocking are one of the main causes that result in the drop of the optical performance of the heliostat fields. In this paper, we suggest through the simulation, an accurate and fast framework to enhance the optical performance of the solar field with the existence of the shading and blocking. By practicing the new style, running down the implementation time and keeping off unnecessary computations, our framework increases the speed of the computations through parallel computing architectures, then using the Artificial Neural Network (ANN) to investigate the efficiency of our proposed system. The results indicate the matching with the previous studies and satisfy the correspondence gain. The results also indicate the optimization of heliostat field layout for 2650 Sener heliostat, which considered as a reference in this work, by using the scarce open literature data on GEMASOLAR (Seville-Spain). Annual efficiency to transform sun's energy to thereceiver has been chosen as the target work. Each mirror position specified using an optimization algorithm, by utilizing the layouts of the MIT team model while two parameters of this model settle down the layout outline of the reflectors.

Keywords: central receiver system; heliostat field; parallel computing; artificial neural networks; shadowing and blocking; phyllotaxis

1. Introduction

The growth in energy demand, the depletion of fossil fuels, and the awareness of the public opinion of environmental problems motivate the production of electrical energy from renewable sources. Sunshine is the most plentiful source of energy on Earth, and every year, the sun delivers more than 10,000 times the quantity of energy that humans currently use [1]. Of all of the technologies for concentrated solar power (CSP), the solar power tower plant (SPTP) technology is viewed as most worthwhile because it has high working temperatures that increase the efficiency of the power cycle. With this great feature and the recent focus on decreasing the price and increasing the efficiency of (SPTP), most researchers have been inspired to work on (SPTP) technology. The primary function is performed by a large number of joined reflectors that are called

the heliostat field, which reflect and condense the rays of the sun toward a main receiver. A computer controls the rotation of each reflector around two axes to ensure a continuous, accurate orientation, with a tracking error of less than a fraction of a degree. By this orientation, the intensified sunlight is focused directly on the tower receiver, where an absorber is heated to temperatures of approximately 1000 °C or more [2]. Heat transfer fluid (HTF) then transfers the absorbed energy to a heat exchanger connected to a gas or steam turbine, which is in its turn coupled to an electric generator. The capital importance and the topic of many studies are the ideal layouts of the reflector field, mainly because the approach requires 50% of the full price of the scheme, and the annual energy loss is approximately 47% [3]. Several codes have been produced for this purpose dating from the 1970s, and most of those codes are

recorded in Ref.[4]. At the same time, the most recent codes[5], [6], [7], [1] mostly use various forms of access for increasing the global efficiency, which is given as:

$$\eta = \eta_{cos} \times \eta_{at} \times \eta_{in} \times \eta_{s\&b} \times \eta_{ref} \quad (1)$$

Where the parameters are the cosine effect efficiency (η_{cos}), the atmospheric attenuation efficiency (η_{at}), the interception efficiency (η_{in}), the shading and blocking efficiency ($\eta_{s\&b}$), and the reflectivity of the heliostats (η_{ref}). The mean yearly heliostat field efficiency or the insolation weighted efficiency ($\eta_{year, Eb}$) is calculated [5] and defined as:

$$\eta_{year, Eb} = \frac{\sum_{day=1}^{365} \int_{sunrise}^{sunset} E_b(t) \eta(t) dt}{\sum_{day=1}^{365} \int_{sunrise}^{sunset} E_b(t) dt} \quad (2)$$

because any (SPTP) optimization operation should depend on the annual energy estimation of the different layouts studied. The annual energy is the integrated sum of the instantaneous energy transformed by all reflectors, over the moments of time [8].

The demand for working out ($\eta_{s\&b}$) with high precision, as time, is high as a rule because the result depends on different factors such as the position of the sun, the position of the reflector, and placement of the neighboring reflectors. At the same time, one of the main ingredients that result in the decline of the optical performance of the heliostat fields must be considered. Thus, during the optimization, all neighbors causing shading or blocking the analyzed reflector should be evaluated individually, to estimate the ($\eta_{s\&b}$) exactly.

Shading often takes place when a heliostat is shaded from the sunlight by an adjoining heliostat or a tower, and blockings similarly occurs if a heliostat blocks the rays of the sun being reflected from an adjoining receiver. Theoretically, high-density heliostat layouts would result in serious shading and blocking and reduce the optical efficiency. Nevertheless, the placement of the mirrors should be equidistant from the tower as much as possible to obtain a high intercept factor. Thus, to optimize the heliostat field layout, the effects of shading and blocking should be computed accurately.

M. Chiesi et al. [1] cut down the computational time through algorithms that utilize a new parallel calculating framework depending on the general objective graphic processing units and carried out on desktop workstations, developed with multiple graphics processing units (GPUs) using the data parallel programming pattern provided by the CUDA C implementation. In addition, the

algorithms for computing the shading and blocking effect based on projection coordinates of the affected heliostats onto the plane are called mirror projection. The main heliostat is then discretized into a matrix of square sub-mirrors. A sub-mirror is counted in the shadow area if the projection of the neighboring mirror falls on it. Similarly to blocking, the only difference is in the observation position, which, in this case, corresponds to the receiver. The model is considered accurate if it has a high number of sub-elements, but this condition also results in slow speed [9], so parallel computing architectures were used in their estimates. Nevertheless, the hurdle of this model is implemented in the normal hardware computing system.

Saeb et al. [7] built on the layout of the MIT team proposed by Noone et al. [5] while at the same time developing the optimization by using genetic algorithm (GA) to find the best value for two parameters, which are considered responsible for the final layout of the field. However, the fixed necessary heliostats (594 of 3000) depend on collected power after considering global efficiency without calculation ($\eta_{s\&b}$). Further, estimation of the annual energy occurred after determining the number of fixed heliostats because the heliostats needed were estimated at noon, March 21st.

In this paper, the central ray tracing and discretization technique was adapted to calculate ($\eta_{s\&b}$) with small subdivisions and high accuracy. However, at the same time, the computational period was ameliorated, and superfluous computations for heliostats that were not causing shading or blocking were blocked, and the process could handle the overlapping problem created by multiple heliostats through using logical parameters. Development of this technique occurred with the use of parallel computing architectures based on the MATLAB Parallel Computing Toolbox, and later by using neural algorithm that clarify in detail. The outcomes are consistent with those of other studies and good improvement in the result is obtained. Then, an optimization study was performed with a new methodology to find the best layout of the field for a GEMASOLAR (SPTP) (Seville –Spain), as a reference used in this work and as a case study [6], utilizing genetic algorithm (GA) and depending on the phyllaxis pattern proposed by Noone [5].

2. Simulation Tools

2.1 The location of the sun

To interpret how to gather energy from the sun, one must first be able to predict the position of the sun with respect

to the heliostats. In this paper, four main necessary solar angle equations have been applied to calculate annual efficiency.

Solar declination(δ): the angle between the earth/sun line and the equatorial plane[10].

$$\delta = 23.45 \sin \left(360^\circ \frac{n_d + 284}{365} \right) \text{ (degree)} \quad (3)$$

Hour angle (ω)[5]for sunrise and sunset estimated from the equation:

$$\omega_{\text{sunrise}} = \cos^{-1}(\tan \phi \tan \delta) - \pi = -\omega_{\text{sunset}} \text{ (rad)} \quad (4)$$

Solar altitude angle(α): the angle between the horizontal plane and light waves coming from the sun[10].

$$\alpha = \sin^{-1}(\sin \delta \sin \phi + \cos \delta \cos \omega \cos \phi) \text{ (rad)} \quad (5)$$

Solar azimuth angle(A): the angular displacement that is measured from due north in a clockwise direction to the earth-sun line projection[11].

$$A = \cos^{-1} \left(\frac{\sin \delta \cos \phi - \cos \delta \cos \omega \sin \phi}{\cos \alpha} \right) \text{ (rad)} \quad (6)$$

Where: if $\sin \omega > 0$, then $A = 2\pi - A$

As noted before, the annual energy reaching the receiver is the total of the instantaneous energy produced by the solid field of heliostats. After transforming the energy from the solar radiation, the moments of time sampled are atypical of the ASHRAE Clear-sky Radiation Model [10], which was utilized to evaluate the solar radiation or beam normal irradiance $E_b(t)$ for (Seville –Spain), as clarified in the ASHRAE Handbook[10].

2.2. Sener heliostats, specifications

GEMASOLAR[12], [6]a power tower plant in (Seville, –Spain), is the plant used as a reference in this work, furthermore, the total dimensions of Sener heliostat and other parameters utilized in GEMASOLAR have been tabulated in Ref [12], [6]. The present study used field parameters are presented in Table 1.

Table1. Gemasolar fields parameters[12], [6]

Heliostats

Width W_h	12.305 m
Height H_h	9.752 m
Heliostat total diagonal, d_h	15.7 m
Heliostat total area, A_h	120m ²
Heliostat mirror area, A_m	115.7 m ²
Effective reflectivity, η_{ref}	0.88×0.95
Heliostat numbers	2650
Receiver	
Tower optical height h_t	140m
Receiver radius R_r	4m
Receiver height H_r	9m
Latitude location, ϕ	37.46 N°(Seville)

2.3. Coordinate transformation of heliostat and discretized heliostat surface

In the selection coordinate system (referred to in the following text as “tower system of coordinates”), east is in the positive(y) direction, and north is in the positive (z)direction, while the zenith is in the (x)direction, as Fig (1) shows.

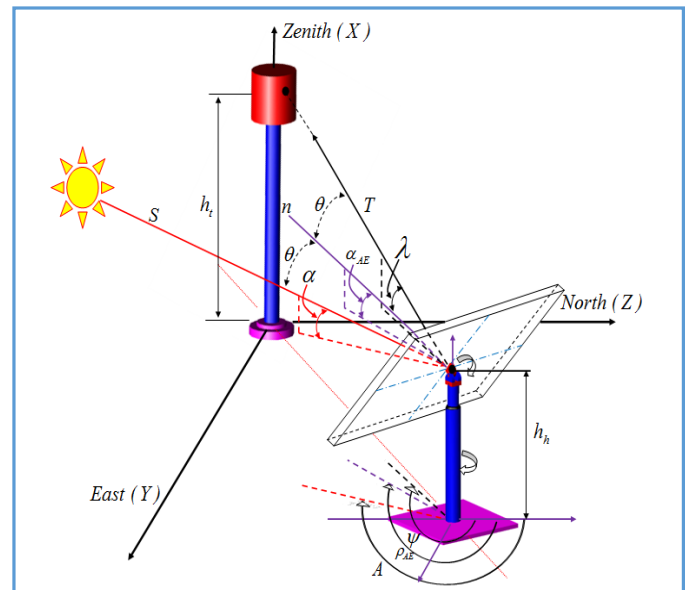


Fig. (1). Coordinate system for heliostat fields attached to the earth-surface reference frame

Given that the sun is a moving object while the receiver is a fixed object, the normal (\vec{n}) of the heliostat has to adjust when the sun position changes with time, to ensure that the heliostat is oriented at the necessary angles. To determine ($\eta_{s\&b}$) of the heliostat, the heliostat position frame

should be estimated. The altered orientation of the frame during the sun tracking period in three-dimensional space can be modelled by applying the coordinate transformation. For the convenience of the three-dimensional coordinate transformation, an additional dimension of space is added to make all of the transformations linear. The rest position or the initial coordinate of the frame is first defined in a fixed coordinate system. When the plane of the heliostat is parallel to the x-y plane, the normal to its surface (\vec{n}) is directed to the north direction, where the center point of the heliostat surface is given by P_C with coordinates (0, 0, 0). In this analysis, the total heliostat surface elements in our research will be 100 because the error reduces to less than 10^{-4} using a grid of 100 points [5], which are assigned for the grid fixed on the moving frame to study the shadow and block effect, as we will see in the following section. The coordinates of the points are treated as a vector in the coordinate space and are written as:

$$P_{i,j} = \begin{bmatrix} P_{i,j,x} \\ P_{i,j,y} \\ P_{i,j,z} \\ 1 \end{bmatrix} \quad (7)$$

In addition, the surface of the heliostat is partitioned into (H_e) number for height (H_h) and (W_e) number for width (W_h), and the diagonal diameter of the element (d_e) which equals $d_e = \sqrt{W_e^2 + H_e^2}$, is calculated. To convert from (P_C) to the center of the discretization area ($P_{i,j}$), we should use translational transformation [T_r, c], which is written as

$$[T_r, c] = \begin{bmatrix} 1 & 0 & 0 & (H_h/2 - ((2 \times i) - 1/2) \times H_e) \\ 0 & 1 & 0 & ((-W_h/2) - ((2 \times j) - 1/2) \times W_e) \\ 0 & 0 & 1 & 0 \\ 0 & 0 & 0 & 1 \end{bmatrix} \quad (8)$$

Then, the coordinates of the center of the discretization area relative to the center of the heliostat is calculated as follows:

$$P_{i,j} = \begin{bmatrix} P_{i,j,x} \\ P_{i,j,y} \\ P_{i,j,z} \\ 1 \end{bmatrix} = [T_r, c] \begin{bmatrix} 0 \\ 0 \\ 0 \\ 1 \end{bmatrix} \quad (9)$$

The reflector is oriented using an actuator for rotation in the coordinate transformation for the Azimuth-Elevation (AE) sun-tracking method [11]. The first rotation transformation by the angle (α_{AE}) about the Y-axis will transform the point from the fixed coordinate system to an elevation-movement coordinate system. The second rotation transformation for the rotational movement by the angle (ρ_{AE}) about the X-axis will transform the point of the elevation-movement coordinate system to the azimuth-movement coordinate system, as shown by the following two rotation matrices, as follows:

$$[\alpha_{AE}] = \begin{bmatrix} \cos(\alpha_{AE}) & 0 & \sin(\alpha_{AE}) & 0 \\ 0 & 1 & 0 & 0 \\ -\sin(\alpha_{AE}) & 0 & \cos(\alpha_{AE}) & 0 \\ 0 & 0 & 0 & 1 \end{bmatrix} \quad (10)$$

$$[\rho_{AE}] = \begin{bmatrix} 1 & 0 & 0 & 0 \\ 0 & \cos(\rho_{AE}) & \sin(\rho_{AE}) & 0 \\ 0 & -\sin(\rho_{AE}) & \cos(\rho_{AE}) & 0 \\ 0 & 0 & 0 & 1 \end{bmatrix} \quad (11)$$

After all of the rotational transformations, the points are transformed from the heliostat coordinate system to the real coordinate system in the heliostat field under a translational transformation [T_r, p] which is written as:

$$[T_r, p] = \begin{bmatrix} 1 & 0 & 0 & h_h \\ 0 & 1 & 0 & E_h \\ 0 & 0 & 1 & N_h \\ 0 & 0 & 0 & 1 \end{bmatrix} \quad (12)$$

The final three transformation matrices for the heliostat [G] are presented as:

$$[G] = [T_r, p][\rho_{AE}][\alpha_{AE}] \quad (13)$$

Finally, the coordinates of the center of the discretization area after finishing the orientation and relative to the coordinate system in the heliostat field, after the transformation ($P'_{i,j}$) are written as:

$$P'_{i,j} = \begin{bmatrix} P'_{i,j,x} \\ P'_{i,j,y} \\ P'_{i,j,z} \\ 1 \end{bmatrix} = [G] \begin{bmatrix} P_{i,j,x} \\ P_{i,j,y} \\ P_{i,j,z} \\ 1 \end{bmatrix} \quad (14)$$

The final matrices are stored in the cells that had previously been set.

3. Methodology and Mathematical Model.

The procedure of an algorithm to estimate the annual optical efficiency of the heliostat field is presented in the flowchart as sketched in Fig. (2). the main step in forming of heliostat field, that

Define field layout, which are based on the pattern of the MIT model[5], which is inspired by the spiral patterns of the phyllotaxis disc. The disc shown increases the overall efficiency of the proposed model. The equations needed for this layout are presented as [5]:

$$\theta_p = 2\pi\varphi^{-2}n_h \quad (15)$$

$$r_p = an_h^b \quad (16)$$

where (θ_p) is the polar position angle for heliostat in field, (r_p) is the radius position for the heliostat, and (a) , and (b) are the layout constants estimated precisely by applying an optimization algorithm later. Further, $(\eta_{year, Eb})$ was considered as the objective function, and all optical efficiency factors were considered, is Estimated according to the Eq. (2). All of the days of the year (1→365) should be considered as shown in Fig. (2). or for comparison with the literature study, specify the 21st of each month during the year, and carry out the discretization model to estimate $(\eta_{s\&b})$ with all computations that are related to the other parameters of optical efficiency, that is clarified in Ref. [6] and [13], during the period from sunrise to sunset.

The shading and blocking function (sbf) calculations are estimated after preparing the final three transformation $[G]$ matrices for the heliostat.

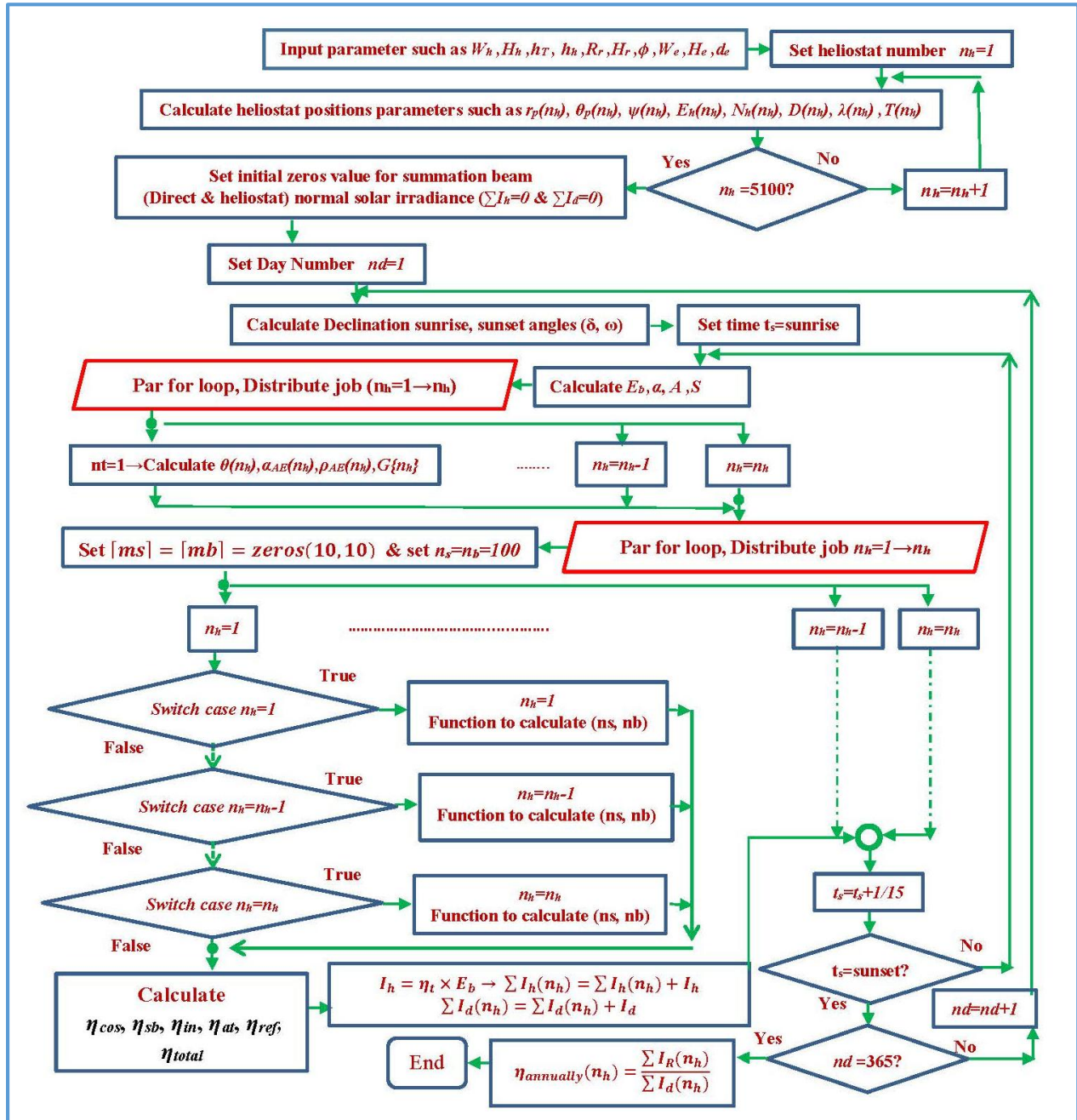


Fig. (2). The flow chart to show the algorithm to estimate the $(\eta_{year, Eb})$

The first step in a function that sets zero matrices as the value of the logic parameters in the shadow and blocking estimate for each number of the heliostats seen in the following form.

$$[ms] = [mb] = \text{zeros}(10,10) = \begin{bmatrix} 0 & \dots & 0 \\ \vdots & \ddots & \vdots \\ 0 & \dots & 0 \end{bmatrix} \quad (17)$$

This matrix is imposed to prevent recalculation of the discretization area that occurs when shadow or block conditions take place with overlapping produced by multiple heliostats. At the same time, the set initial value for the number of discretization areas for calculating shading and blocking is $(ns = nb = 100)$. In the beginning, the numbers of the heliostats causing (n_{sb}) have been fixed, which probably causes shadowing and blocking, and named (heliostat causes) for shadowing and blocking, then finding polar coordinates $(r_{sb} \& \theta_{sb})$ of each relative to the main heliostat and studying the

effect of each reflector on the main heliostat separately. As an example, we have a heliostat number (571), which is seen in Fig. (3). This method may lead to the selection of heliostats that is more than factual. Study heliostats also might not have an impact on the shading and blocking effect at the specified time. So, the next steps will include estimation of the possibility for each heliostat, whether the shading or blocking is affected or not before the calculation of $(\eta_{s\&b})$. If the shading or blocking has not been impacted, the heliostat should be passed and another heliostat studied. In this way, we can decrease the time for computation by decreasing a number of heliostats that will require implementation $(\eta_{s\&b})$ computations. Then, prevent any overlapping produced by multiple heliostats in the calculations, and the computation can be done with tests, which are summarized in the next points.

1- Testing between the heliostat main and the heliostat causes if the intersection between the horizontal circles of the movement exists, and it can be done, by a comparison between diagonal diameters.

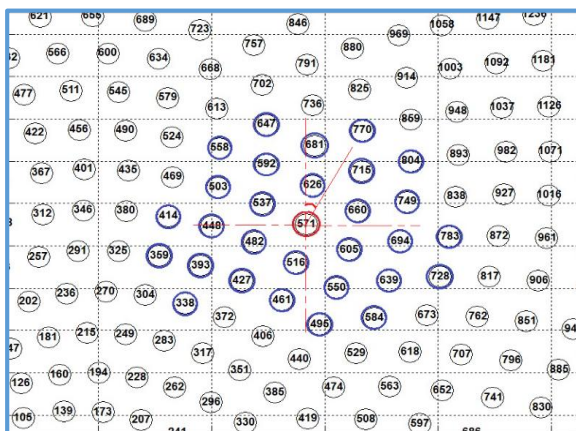


Fig. (3). Fixed heliostat numbers that cause shadowing and blocking for heliostat (571), with the polar coordinates $(r_{sb}$ and $\theta_{sb})$

2-Shadowing and blocking aperture:

The shadowing aperture is a window that allows the sunshine to fall on the main heliostat through it. Any obstacle (heliostat) in the place of the direction of the rays of the sun will cause shadow to occur on the main heliostat. The shadowing aperture can be seen as a thick red line in Fig.(4). The chance of an event should be checked in this case, depending on the solar azimuth angle A , when the (θ_{sb}) value is within the possible range of angle $A, (\pm 90)$. The blocking aperture is a window that passes sunshine through, from the main heliostat toward the tower. Any obstacle (heliostat) in the direction of the rays of the sun will cause blocking to occur on the main heliostat. Check the chance of an event in this case, depending on the heliostat polar angle or facing angle $\psi(n_h)$ which is seen in Fig.(1),

when the θ_{sb} value has been within the possible range of angle $\psi(n_h), (\pm 90)$.

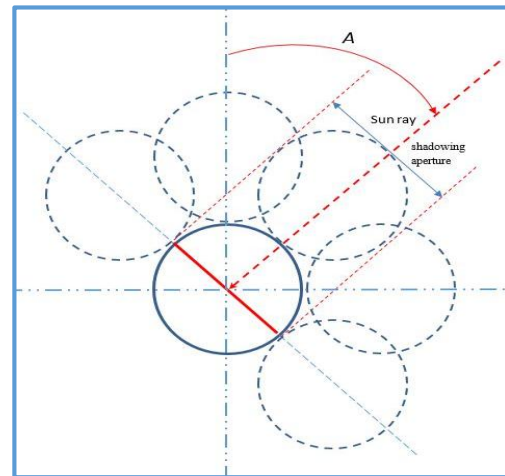


Fig. (4). Shadowing aperture

3- Normal distance between the two centers of the circles of movement of the heliostats (main heliostat and heliostat causes), which is presented here as (P_1, P_2) . For shadowing, the normal distance (d_{s1}) between the center of the circle of movement for each heliostat cause and the vector of the sun that passes through the center circle of movement of the main heliostat should be calculated [14] from the following equation.

$$d_{s1} = \frac{\| \overrightarrow{P_1 P_2} \times \vec{S} \|}{\| \vec{S} \|} \tag{18}$$

Then, a comparison is made between distance (d_{s1}) and diameter of movement (d_h) for each heliostat. If the distance falls within the circle of movement of the heliostat causes, shadow occurs. For blocking; the normal distance (d_{b1}) between the center of the circle of movement for each heliostat and the vector of the tower that passes through the center of the circle of movement of the main heliostat should be calculated [14] from the following equation.

$$d_{b1} = \frac{\| \overrightarrow{P_1 P_2} \times \vec{T} \|}{\| \vec{T} \|} \tag{19}$$

Then, a comparison is made between distance (d_{b1}) and diameter of movement (d_h) for each heliostat as the shadow case. After passing the likelihood test for shadowing and blocking those have been set for heliostat causes and having confirmed that heliostat causes have an impact by shadowing

and blocking, then divide the heliostat causes and main surfaces into 100 elements, as shown in Fig. (5).

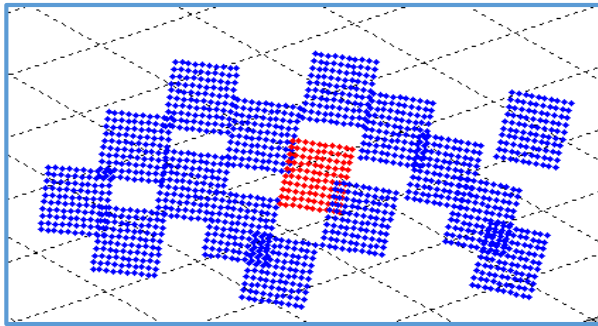


Fig. (5). Discretization area of heliostats

Then, find the coordinates of the center of the discretization ($P'_{i,j}$) of the heliostats (causes and main) relative to the coordinate system in the heliostat field after the transformation by using Eq. (14). After that, by using the same Eq. (18) for shadowing. The normal distance (d_{s2}) is found between the center of the subdivisions ($P'_{i,j,sb}$) of each heliostat cause and the center of the subdivisions ($P'_{i,j,h}$) of the main heliostat that the vector of the sun passes through. Later, a comparison is made between the distance (d_{s2}) and the diagonal diameter (d_e) of the subdivisions. If the distance falls within the diagonal diameter, shadowing occurs. Then by using the same Eq. (19), for blocking, the normal distance (d_{b2}) is found between the center of the subdivisions ($P'_{i,j,sb}$) of each heliostat cause and the center of the subdivisions ($P'_{i,j,h}$) of the main heliostat that the vector of the tower passes through. Then, same comparison is made between the distance (d_{b2}) and the diagonal diameter (d_e) of the subdivisions; as Fig. (6) shows.

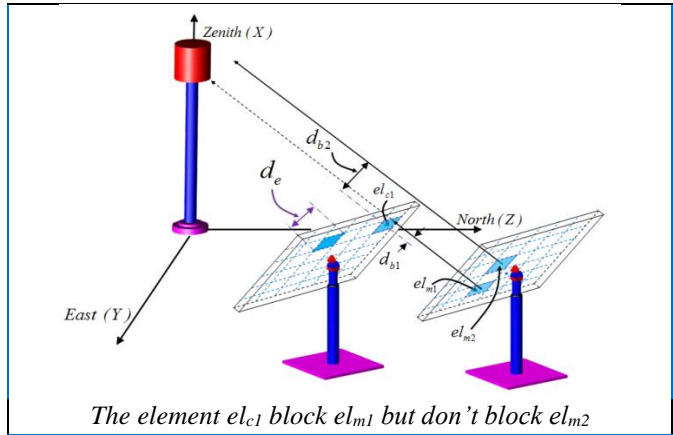


Fig. (6). Normal distance between two centers of subdivisions

At the same time, after confirmation that the subdivision of the main heliostat is affected by shadowing or blocking. The value of the number of discretization areas (ns or nb) is decreased one unit, and the value of the element in the zero matrices, from imposing Eq. (17) as a logic parameter (in the case of shadowing ($ms(i,j)$) and case blocking ($mb(i,j)$) that have the same position ($P'_{i,j,h}$) in the arrangement subdivision of the main heliostat is changed to one. Finally, to calculate ($\eta_{s\&b}$), we should estimate the area that is not effected by shadowing and blocking, and we can do that by multiplying (ns, nb) by the area of an element as follows:

$$A_s = n_s * A_e \quad (20)$$

$$A_b = n_b * A_e \quad (21)$$

Then, the shadowing efficiency is calculated as follows:

$$\eta_{shadow} = \frac{A_s}{A_t} \quad (22)$$

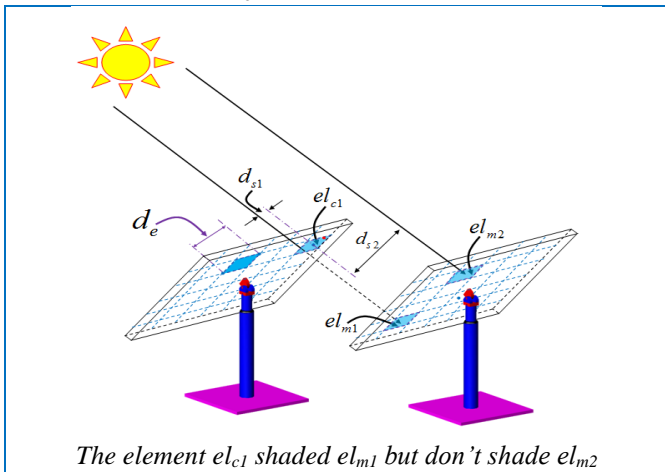
Then, the blocking efficiency as follows:

$$\eta_{block} = \frac{A_b}{A_t} \quad (23)$$

This technique is characterized as an accurate model but at the same time, the slowest model, so one of the targets of this study is how to use this technique, or its accuracy calculation, with less implementation time.

The first solution to decreasing processing time is that for each step of time, parallel computing is carried out to perform all computation that is related to factors of annual efficiency.

As scientific/engineering problems grow in complexity and the need for computational and storage resources grows,



Therefore, The second step to speed up operations while keeping high accuracy in calculations is the use of fast algorithms, the ANNs used. ANNs feature a relative simplification of a simulation methodology description. Neural networks are employed to find out the manner of the system and then to simulate and anticipate its manner. ANNs, although carried out on computers, are not programmed to do specific jobs. Instead, the ANNs are trained on data sets until they learn the patterns used as inputs. Once the ANNs are trained, new patterns may be delivered to them for prediction or classification. ANNs can automatically learn to spot patterns in data from real systems or physical examples, computer programs, or other authors. They can handle many inputs and obtain results in a shape suited for architects. A training set is a group of matched input and output patterns used for training the network, usually by suitable adjustment of the synaptic weights. The outputs are the dependent variables that the network produces for the corresponding input. It is important that all the information the network needs to learn be supplied to the network as a data set. When each pattern is read, the network uses the input data to produce an output, which is then compared to the training pattern, i.e., the correct or desired output. If there is a difference, the connection weights (usually, but not always) are altered in such a direction that the errors decreased. In this paper, the task of the ANNs is to estimate $(\eta_{\text{sh}} \& \eta_{\text{bl}})$, which depends on the location of the sun and the heliostat location, after fixing the location of the neighboring heliostat when the (GA) finds the best layout from the previous step. Therefore, in our code, the input and output variables for ANNs are presented in Table (2).

Table 2. Input and output variables for ANNs

Input variables	
1	Solar declination δ
2	Solar altitude angle α
3	Solar azimuth angle γ
4	Polar angle for heliostat axis position θ
5	ρ Radius position for heliostat ρ
Output variables	
1	Shadowing efficiency η_{sh}
2	Blocking efficiency η_{bl}

In addition, the training set is prepared during runs of the code for each fixed time step (specific period of days during the year and specific period of minutes during the day), which will be presented in the next section. By recording the input and output variables, which are used for training the network, and

detecting suitable adjustments of the synaptic weights, we will identify the network type that was used: generalized regression with one hidden layer and one output layer as shown in Fig. (7). Then, after preparing the network of ANNs, the ANNs are joined with the main code instead of the shading and blocking function $(\eta_{\text{sh}} \& \eta_{\text{bl}})$ and transformation matrices (G), to use the ANNs in computations of efficiency.

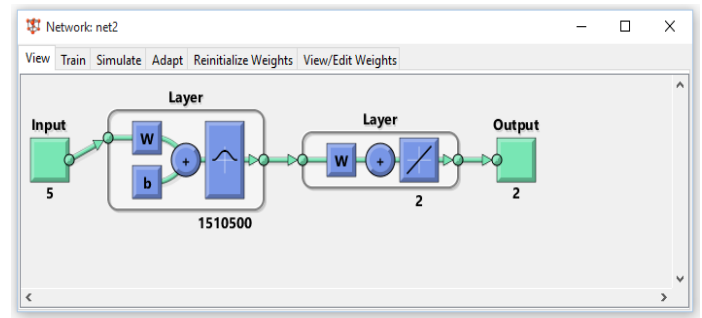


Fig. (7). Properties of the network, which is used in ANNs

6. Computational Benchmarking

The first comparison targets the performance of computing $(\eta_{\text{sh}} \& \eta_{\text{bl}})$ by ANNs, and compares results with a discretization model with parallel computing.

First, it is necessary to adjust fixed time steps to ensure the validity of the results at the lowest errors and high resolution, which is used to prepare a training set, found during the runs of the code for each fixed time step.

As Table (3) shows, errors occur in the calculation of $(\eta_{\text{sh}} \& \eta_{\text{bl}})$ when multi-values of the time step are used. Increases in the steps or decrease in the duration time during training leads to higher accuracy in evaluating the $(\eta_{\text{sh}} \& \eta_{\text{bl}})$. An acceptable error is therefore imposed at 10^{-2} when used (15 days and 20 minutes).

Table 3. Calculation error in the $(\eta_{\text{sh}} \& \eta_{\text{bl}})$ as a function of fixed time step

Minute / day	30	15	5
32	10^{-1}	10^{-1}	10^{-1}
20	10^{-1}	10^{-2}	10^{-3}
10	10^{-1}	10^{-3}	10^{-4}

The performance of the network and the instantaneous error (that is, single time step) in calculating $(\eta_{\text{sh}} \& \eta_{\text{bl}})$ by ANNs can be seen in Fig. (8), when several days are studied randomly during the year. Then, one day is chosen randomly, its sequence equal to 180, not within the days on which the network was trained to present the result that is based on computing $(\eta_{\text{sh}} \& \eta_{\text{bl}})$ during the day, from sunrise to sunset and

every four minutes. A period is selected, different from the period fixed when the network was trained. The convergence noted between the results is shown in Figure Fig. (8).

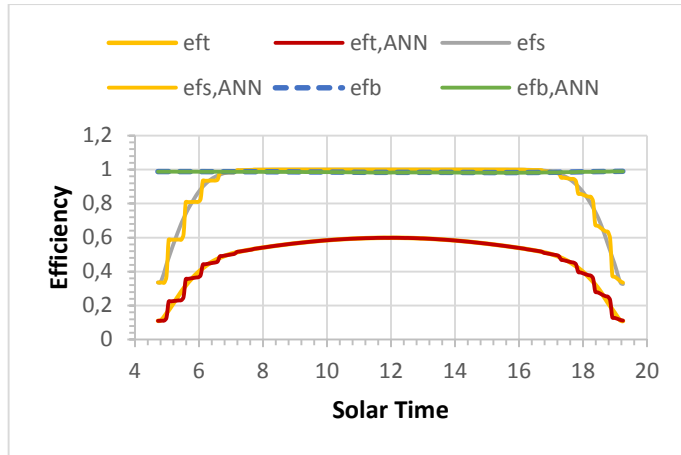


Fig. (8). Deferent between ANNs and the discretization model, for computing the field efficiency (eft) and shadow efficiency (efs) and block efficiency (efb), for day 180 and every 4 minutes

Further, Table (4) shows the total values of efficiencies and for all field, for ANNs and the discretization model, throughout the day.

Table 4. The values of efficiencies during the day

	Field Efficiency	Shadow Efficiency	Block Efficiency
ANNs	0.539321	0.97353	0.984169
Discretization Model	0.539909	0.97457	0.984228

Two heliostats from the field (2640, 3006) are chosen and used to study ANNs performance, as seen in Fig. (9), which presents their position as a red circle inside the figures

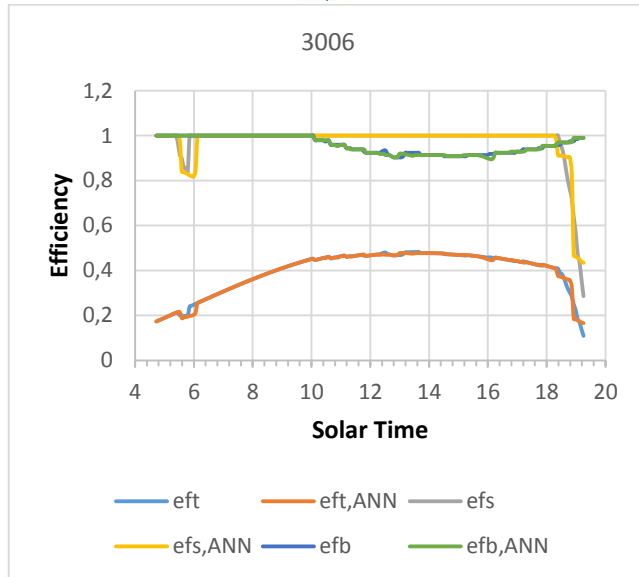
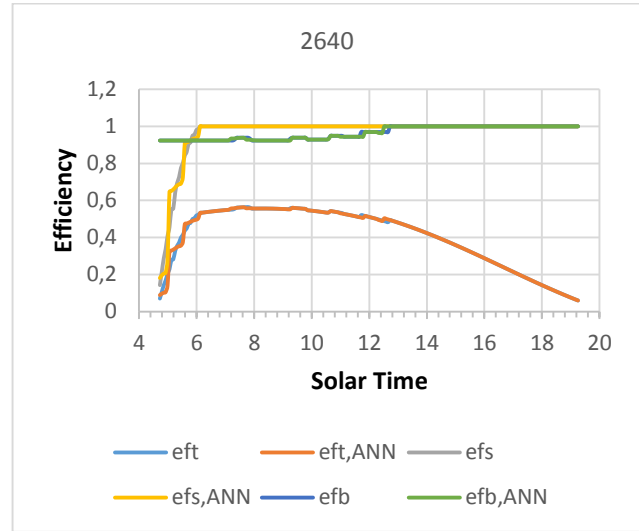


Fig. (9). Deferent between ANNs and discretization model for computing efficiencies for heliostats (2640,3006)

Additionally, the implementation time for one- step has been reduced to 191.79 sec as shown in Table (5).

Table 5. The values of the implementation time (sec) for one-step for the deferent technique

Discretization Model without Parallel	Discretization Model with Parallel	ANNs without Parallel	ANNs with Parallel
16750.045	2640.2844	573.909	191.79

factors are responsible for the scheme of the layout of the field, and these factors are handled as the forming variables, where the best values are estimated by using an optimization algorithm while improving the annual efficiency (η_{annual}) when chosen as a target. Benchmarking with the previous study, a clarified higher efficiency than that estimated by others, and displaying the new model can estimate the (η_{annual}) precisely with a low implementation time

References

- [1] Chiesi, M., Vanzolini, L., Scarselli, E.F., Guerrieri, R. Accurate optical model for design and analysis of solar fields based on heterogeneous multicore systems, *Renewable Energy* 55 (2013) 241-251.
- [2] Leonardi, E, D'Aguanno, B., CRS4-2: A numerical code for the calculation of the solar power collected in a central receiver system.; *Energy* 36 (2011) 4828-4837.
- [3] Wei, X., Lu, Z., Yu, W., Wang, Z., A new code for the design and analysis of the heliostat field layout for power tower system, *Solar Energy* 84 (2010) 685-690.
- [4] Garcia, P., Ferriere, A., Bezia, J.-J., Codes for solar flux calculation dedicated to central receiver system applications: A comparative review, *Solar Energy* 82 (2008) 189-197.
- [5] Noone, C.J., Torrilhon, M., Mitsos, A., Heliostat field optimization: a new computationally efficient model and biomimetic layout. *Solar Energy* 86 (2012) 792-803.
- [6] Collado, F.J., Guallar, J., A review of optimized design layouts for solar power tower plants with campocode; *Renewable and Sustainable Energy Reviews* 20 (2013) 142-154.
- [7] Besarati, S.M., Goswami, D.Y., A computationally efficient method for the design of the heliostat field for solar power tower plant. *Renewable Energy* 69 (2014) 226-232.
- [8] Collado, F.J., Guallar, J., Campo: generation of regular heliostat fields. ; *Renewable Energy* 46 (2012) 49-59.
- [9] Weidong H., Longlong L., Yongping L., Zhengfu H., Development and evaluation of several models for precise and fast calculations of shading and blocking in heliostats field, *Solar Energy* 95 (2013) 255-264.
- [10] ASHRAE Handbook. American Society of Heating, Refrigerating and Air-Conditioning Engineers; 2013 ASHRAE Handbook - Fundamentals (SI); CLIMATIC DESIGN INFORMATION.
- [11] K.K. Chong, M.H. Tan, Range of motion study for two different sun-tracking methods in the application of heliostat field; *Solar Energy* 85 (2011) 1837-1850.
- [12] Burgaleta, J.I., Arias, S., Ramirez, D. (2011) GEMASOLAR: the first tower thermo-solar commercial plant with molten salt storage. SolarPA-CES 2012 International Conference.
- [13] Schmitz, M., Schwarzbozl, P., Buck, R., Pitz-Paal R. Assessment of the potential improvement due to multiple apertures in central receiver systems with secondary concentrators. *Sol Energy* 80 (2006) 111-20.
- [14] Gerald Farin & Dianne Hansford, "Practical Linear Algebra: A Geometry Toolbox," Third edition. © 2014 by Taylor & Francis Group.
- [15] Jeremy Kepner. Parallel MATLAB for Multicore and Multinode Computers, QA76.58.K46 2009.